Comparison of x-ray absorption with x-ray photoemission of nickel dihalides and NiO

G. van der Laan, J. Zaanen, and G. A. Sawatzky
Physical Chemistry Department of the Materials Science Center, University of Groningen, Nijenborgh 16, 9747 AG Groningen, The Netherlands

R. Karnatak and J.-M. Esteva
Laboratoire pour l'Utilisation du Rayonnement Electromagnetique, Université Paris—Sud, Bâtiment 209 C, F-91405 Orsay Cédex, France
(Received 26 September 1985)

High-resolution $L_{2,3}$ x-ray absorption data are presented for nickel dihalides and nickel oxide. The near-edge multiplet splitting is observed to decrease rapidly with decreasing anion electronegativity. This decrease is accompanied by an increase in a satellite feature. A detailed analysis of the data in terms of recently proposed many-body theories is presented and is shown to yield excellent agreement with experiment allowing a determination of the charge-transfer energy, the d-d Coulomb interaction, and the Ni d—anion p hybridization interaction. We show that the values obtained are in good agreement with those obtained from x-ray photoelectron spectroscopy even though the spectral shapes are strongly different. The difference in spectral shapes is shown to be due to the very different final states.

I. INTRODUCTION

Transition-metal compounds have been an interesting and controversial topic of research since 1937, when it was pointed out[1] that divalent Ni compounds like NiO have large band gaps, whereas one-electron band theory[2] predicts them to be metallic. The introduction of the concept of electron correlation by Mott[3] in 1949 that at least qualitatively explains the band gap was the beginning of a controversy concerning the magnitude of the d-d Coulomb interaction, which has apparently not yet been solved to everyone's satisfaction. Recent sophisticated band-structure calculations still predict at most a small (0.3 eV) gap for NiO,[4,5] whereas modern direct experimental determinations of the gap yield 4.3 eV.[6,7] The problem is, in fact, much more general than only NiO. Band-theory calculations of the Ni dihalides all predict metallic behavior or, at most, a small band gap, whereas optical measurements suggest a large band gap decreasing with decreasing electronegativity of the anions.[8] This and also cluster calculations on NiO and $NiCl_2$ (Ref. 9) suggest that the band gap is more like a charge-transfer gap than a d-d gap. This is in qualitative disagreement with band theory and also in disagreement with the Mott-Hubbard theory when considered in the simplest sense. The interpretation of the valence-band spectroscopies in terms of the cluster theory leads to the experimentally observed 30-eV spread in d spectral weight in NiO provided the d-d Coulomb interaction is around 7—9 eV.[6,10] Important for us here is that the same cluster theory can also be used to interpret core-level spectroscopies providing a unified approach. This was demonstrated by us some time ago for the Cu dihalides[11] and Ni dihalides.[12] The importance of core-level spectroscopies in this is that they provide an independent measure of the various parameters occurring in the theory.

Recently, we have extended the cluster theory to include the anion p bandwidths and have shown that the observed trends in band gaps for the transition-metal compounds, including both insulators and metals, can be understood in a quite natural manner.[10] The same theory has been used to explain in detail the highly structured Ni $2p$ core-line x-ray photoelectron spectroscopy (XPS) spectra of the Ni dihalides, from which we have obtained the relevant parameters for describing the valence-band structure.[13] In this paper we show that the same theory can be used to describe new high-resolution x-ray-absorption spectra in great detail, providing another independent measure of the parameters.

As pointed out previously,[14] x-ray-absorption spectroscopy (XAS) has several advantages over XPS, and the various interactions and hybridization enter into the XAS problem in a different way, making it complementary to XPS. The differences between XPS and XAS are twofold. First, in XPS the initial ground-state valence electrons experience the full potential of an unscreened core hole, whereas in XAS the core electron can be excited into an efficient screening orbital so that the perturbation on the remaining ground-state electrons is small. Second, in XPS the various components of the spectrum are broadened by multiplet structure rather than exhibiting specific multiplets, because virtually all of the many final-state multiplets can be reached. XAS, by virtue of the dipole selection rules, is, on the other hand, quite selective in multiplet structure. Only a limited number of states are accessible and therefore become visible as separate structures in the spectrum. As we will show below, the multiplet splitting itself can then be used to provide information on the various interactions.

The paper is organized as follows. In Sec. II we present

the experimental results and describe the techniques used. In Sec. IV we present the theory applied to the x-ray-absorption problem. In Sec. V we present a comparison of theory and experiment and obtain values for the charge-transfer energies, *d-d* Coulomb interaction, and hybridization interactions, and we compare these to previous values obtained with XPS.[13]

II. EXPERIMENTAL DETAILS

X-ray-absorption data were taken using the synchrotron radiation emitted by the Anneau de Collisions d'Orsay (ACO) using a constant-deviation double-crystal monochromator equipped with beryl crystals. The resolution for this instrument is 0.35 eV.[15] Checks were made on the light flux from the monochromator using Al, which has a flat absorption in the energy of interest here. The energy scale was calibrated by setting the La $2p_{1/2}$ and Mg $1s$ edges to an energy of 850.5 and 1303 eV, respectively. The spectra were recorded by the photoyield method in a vacuum of 10^{-9} Torr or better. NiI_2, $NiBr_2$, and $NiCl_2$ were prepared by subliming— *in situ*—at temperatures around 600—700 °C on an Al plate. NiF_2 was measured as a powder. The absorption spectra taken immediately after sublimation were always identical to the spectra taken after several hours.

III. RESULTS

The experimental results for the Ni dihalides are shown in Fig. 1. The spectra are corrected for a linearly increasing background. We note that in NiI_2 the I $3p_{3/2}$ edge is near the Ni $2p_{1/2}$ structure. In the spectra two main groups of peaks due to the $2p_{3/2}$ and $2p_{1/2}$ edges can be distinguished. In Table I the absolute energies of the first line in the $2p_{3/2}$ and $2p_{1/2}$ edges are given together with the relative energies of the subsequent structures. As can

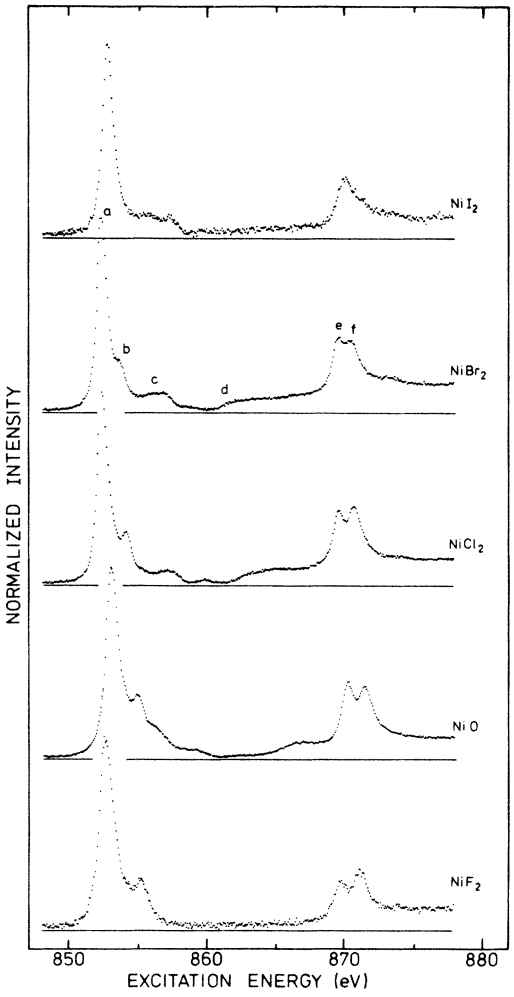

FIG. 1. $L_{2,3}$ absorption spectra of Ni compounds. The L_3 (L_2) edge is found at about 852 (870) eV.

TABLE I. Absolute energies (eV) of the first peak in the XAS $2p_{3/2}(L_3)$ and $2p_{1/2}(L_2)$ edges in the Ni compounds, and the energy separations of the subsequent features. The XPS $2p_{3/2}$ threshold peak positions for the dihalides are given for comparison.

Type of configuration	Peak in Fig. 1	NiI_2	$NiBr_2$	$NiCl_2$	NiO	NiF_2
XAS						
$2p_{3/2}3d^9$	*a*	852.8	852.6	852.7	853.2	852.7
	b	0.5	1.3	1.7	1.9	2.7
$2p_{3/2}3d^{10}\underline{L}$	*c*	2.9	3.5	4.4	5.6	
		4.6	4.4	5.2	6.2	
$2p_{3/2}3d^9\underline{L}k$			6.5	7.3		
	d		9.0	10.0	13.0	
$2p_{1/2}3d^9$	*e*	870.1	869.7	869.8	870.3	869.8
	f	0.5	1.0	1.1	1.2	1.4
XPS						
$2p_{3/2}3d^9\underline{L}$		853.4	854.7	855.6		857.0

be seen, the spectra display a strong variation on chemical environment. Almost all intensity goes into the two white lines a and b, respectively, e and f (Fig. 1). The separation between these peaks decreases strongly (by as much as 2 eV) on going from the fluoride to the iodide.

In all compounds, except NiF_2, a broad satellite is observed at about 4.5 eV above the $2p_{3/2}$ edge (peak c). This satellite has an intensity of roughly 7% relative to the $2p_{3/2}$ white lines. In $NiBr_2$ and $NiCl_2$ another tiny feature proceeds the onset of a continuum (d).

In the $2p_{1/2}$ structure the separation between the white lines is smaller, but the trend that this separation reduces in going toward the iodide is maintained. The satellite structure and the onset of the continuum above the $2p_{1/2}$ edge mimics that of the $2p_{3/2}$ edge, but they are broader and therefore less visible (Fig. 1) and for this reason not tabulated.

Before we discuss the theoretical model, we summarize here some of the features which we wish to address. For comparison purposes we also include in Table I the binding energies as obtained from XPS measurements. Comparison of the threshold peak position in XPS and XAS shows that whereas the XAS energies are only slightly compound dependent, those in XPS are strongly compound dependent. Also, the XPS energies are considerably larger than those found in XAS. This is qualitatively consistent with our previous remark that in XPS the screened threshold peak must result from a redistribution of ground-state electrons. Such a redistribution always costs energy in insulating materials of an amount comparable to the band gap or rather the ionization potential relative to the Fermi level of the valence electron, used for the screening. In XAS the screening is done by the excited electron and therefore we expect the binding energies to be lowered by roughly the band-gap energy. The trend observed in XPS and XAS threshold energies follows nicely the trend seen in optical spectroscopies of the charge-transfer energy and the trend predicted for the band gap in a recently presented theory.[10]

Whereas in XPS we observe two strong satellite lines at about 5 and 9 eV from threshold, there is only a low-intensity satellite (marked c in Fig. 1) in the XAS spectrum. This also is qualitatively consistent with the previous statement that in XPS the ground-state electrons must do all the screening, whereas in XAS it is done to a large extent by the excited electron.

Also different in XAS is the two-peaked structure at threshold which can qualitatively be explained by the multiplet structure and optical selection rules for transitions from a $d^8(^3A_{2g})$ to the $2\underline{p}d^9$ multiplets.[16] However, the observed trend in splitting for the compounds will have to be explained by the theory.

In addition to these differences, which we will treat in detail in the subsequent theory, there are two features, namely the continuum onset (d) and the very weak peak between c and d visible in $NiCl_2$, which deserve separate attention since they involve transitions to the Ni $4s$—like band.

IV. THEORY

To explain the above-mentioned features, we first recognize that the divalent Ni ions in all the compounds studied are in nearly octahedral coordination of nearest-neighbor anions. In the resulting O_h point group the crystal or ligand fields together with the d-d Coulomb and exchange interactions result in a ground state of $^3A_{2g}(e_g^2)$ symmetry for a d^8 electronic configuration. In such a completely ionic model the anions obtain a noble-gas configuration with a completely filled valence p shell. The Ni core $2p \rightarrow 3p$ absorption spectrum in this case would be relatively simple since we merely have to calculate the multiplet structure of a p^5d^9 configuration, taking into account the atomic spin-orbit coupling, the $2p$-$3d$ and $3d$-$3d$ Coulomb interactions, and the crystal-field interaction, and calculate the optical transition probabilities from a $^3A_{2g}(e_g^2)$, ground state. This calculation has been published previously[16,17] and we refer to these papers for details. For the calculation of atomic values for the various Slater and exchange integrals, as listed in Table II, an effective $2p$ spin-orbit splitting of 17 eV and a crystal-field splitting of $10Dq = 1.5$ eV were used.[18]

In Fig. 2 we compare this calculation to the XAS spectrum of NiF_2. This is the most ionic of all the compounds and thus is expected to resemble closely the above free-ion calculation. Indeed, we find close agreement and see that the threshold structure in both the $2p_{3/2}$ and $2p_{1/2}$ regions is due to multiplet structure. It appears, therefore, that hybridization effects in NiF_2 are rather small, or at least not detectable in XAS. From the previous XPS results[13] we observed quite large satellite structure due to hybridization, which appears to contradict the present results. However, as stated above, XPS is quite different from XAS and is, especially in systems like

TABLE II. Values for Δ and the $3d^8$, $3d^9$, and $3d^{10}$ characters in the ground state and for U as obtained from a best fit to an impurity model. Additional constants for all compounds: $Q = 7$, $T = 1.5$ (1.75 in NiO), $W = 3$, $10Dq = 1.5$, $G^1 = 5.79$, $F^2 = 7.72$, $G^3 = 3.29$ eV, the effective spin-orbit splitting is 17 eV, the intrinsic line width is a 0.3-eV Lorentzian, the experimental resolution is a $\sigma = 0.3$ eV Gaussian.

	Δ (eV)	$3d^8$	$3d^9$	$3d^{10}$	U (eV)
NiI_2	1.5	0.47	0.44	0.09	4.5
$NiBr_2$	2.6	0.61	0.32	0.07	5
$NiCl_2$	3.6	0.71	0.23	0.06	5
NiO	4.6	0.73	0.21	0.06	5
NiF_2	7	~ 1.0	~ 0	~ 0	

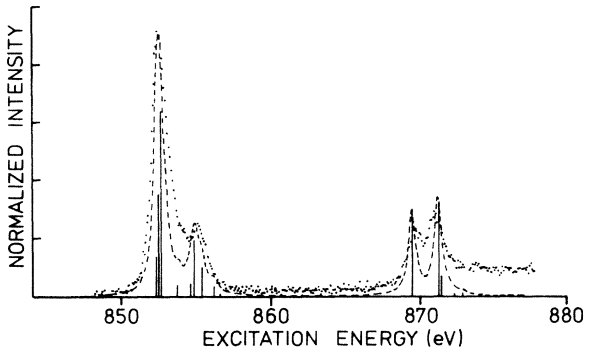

FIG. 2. Calculated multiplet structure for a dipole transition Ni $3d^8 \rightarrow 2p^5 3d^9$ ($G_1 = 5.79$, $F_2 = 7.72$, $G_3 = 3.29$, and $10Dq = 1.5$ eV); the dashed line is a convolution by a 0.6-eV full width at half-height (FWHH) Lorentzian. For comparison, the experimental $L_{2,3}$ spectrum of NiF_2 is shown (dots).

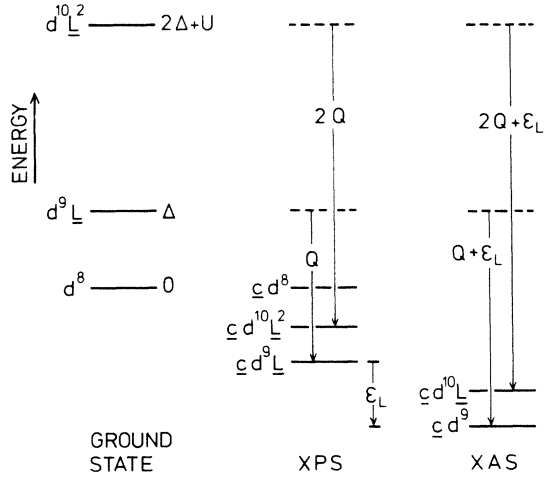

FIG. 3. Energy-level scheme for (a) the ground state, (b) the XPS final states, and (c) the XAS final states.

these, very sensitive to hybridization in the core *final* state, as we will demonstrate below.

The apparent reduction of the multiplet splitting and the appearance of a broad satellite in the other compounds is most likely a result of hybridization. This can be treated in various degrees of sophistication. The simplest way is to postulate that hybridization with anion states causes an effective reduction of the Slater integrals and therefore the multiplet splitting. Although the multiplet splitting change with compound can be explained in this way, one misses the relevant physics involved. First of all, the reduction is caused by hybridization in the *final* state and should not be confused with covalency in the *initial* state. The final and initial state hybridizations are, as we will show below, quite different. Second, one cannot explain in this way the satellite structure, which, although weak, also has its origin in hybridization effects and therefore should be treated on an equal footing as the change in multiplet splitting.

A better approximation is to use a cluster approach in which one calculates the spectrum of a central Ni ion hybridizing with a nearest-neighbor shell of six anions. This cluster approach has been successfully used in the interpretation of XPS spectra of Cu dihalides[11] and Ni dihalides,[12] as well as valence-band and optical spectra in compounds of Cu,[19] Ni,[9,13] and Ce.[20,21] The approximation made here is that the translational symmetry in the solid is assumed to be of minor importance and therefore the one-electron dispersional part of the bandwidths is neglected. This, as we pointed out recently,[10] is probably a good approximation for the d bands since their dispersion width is only about 0.5 eV,[8] which is certainly much smaller than the atomic d-d Coulomb and exchange interactions. However, the anion valence p bands have a considerable dispersion, resulting in widths of 3–4 eV,[8] and this certainly is not negligible compared to hybridization energies and experimental resolution, so it is important to include the anion p bandwidth in the theory.

Before we do this more complicated theory, we turn back to the cluster model since it embraces most of the relevant physics and is more transparent in discussing the qualitative features of the results and the physical origin of the various parameters which enter into the problem. To calculate the core-hole XPS or XAS spectrum, we need to know the ground-state wave function and the core-hole final eigenstates. In the cluster approach we calculate the ground state of a $(NiL_6)^{4-}$ cluster for the dihalides with a basis set of states d^8, $d^9\underline{L}$, and $d^{10}\underline{L}^2$, where $\underline{L}$ is a combination of ligand p wave functions of the appropriate symmetry which has been discussed previously.[9,19] The parameters entering the calculation are the charge-transfer energy Δ, the d-d Coulomb interaction U, and the d-L transfer integral T. Of these parameters only Δ is strongly anion dependent, being given roughly by the electronegativity difference between anion and cation.[11] The energy-level scheme is shown in Fig. 3, which also defines the parameters. In principle, the calculation must be done for every irreducible representation of the O_h point group spanned by a d^8 configuration to find the lowest-energy state. However, we know that the crystal-field and the Coulomb and exchange interaction ensure that the $^3A_{2g}$ irreducible representation determines the ground state. The appropriate $d^9\underline{L}$ and $d^{10}\underline{L}^2$ states of $^3A_{2g}$ symmetry are discussed in detail in a previous paper.[12] The ground-state wave function is then of the form

$$\Psi_0(^3A_{2g}) = \alpha_0 | d^8 \rangle + \beta_0 | d^9\underline{L} \rangle + \gamma_0 | d^{10}\underline{L}^2 \rangle , \qquad (1)$$

where the coefficients and ground-state energy are determined by diagonalizing the Hamiltonian matrix

$$H = \begin{vmatrix} 0 & T\sqrt{2} & 0 \\ T\sqrt{2} & \Delta & T\sqrt{2} \\ 0 & T\sqrt{2} & 2\Delta+U \end{vmatrix} . \qquad (2)$$

As explained previously, the $\sqrt{2}$ arises from the degeneracy of the $d^8(^3A_{2g})$ configuration. From the energy-level diagram in Fig. 3, we see that the ground state has predominantly d^8 character.

Neglecting first of all the final-state multiplet structure but including the core-hole—d-electron Coulomb attraction (Q), we can also calculate the final-state eigenfunctions and energies for both XPS and XAS. The energy-level diagram for these is also shown in Fig. 3 and is

drawn for $Q>\Delta>Q-U$, as is often the case for Ni compounds. From this diagram alone one can immediately see the difference in XPS and XAS. First, in XPS there are three final states resulting in a three-component core-line spectrum, whereas in XAS only two final states are present, resulting in a two-component spectrum. Also, in XPS the ordering of levels is different from that in the ground state, resulting in large satellite intensities. In XAS, on the other hand, the ordering of levels is the same as that in the ground state (after adding one d electron) and, therefore, satellite intensities are expected to be small. In fact, if $Q=U$ there will be no satellite line in XAS since both the ordering and spacing of levels is the same as in the ground state with one d electron added.

We see also from Fig. 3 that the XPS threshold state is primarily of $\underline{c}d^9\underline{L}$ character, while that of XAS is mainly $\underline{c}d^9$. The energy difference between these states is just the ligand ionization potential ε_L, which decreases in going from the fluoride to the iodide. This is the trend observed in the difference between XPS and XAS threshold lines as given in Table I. Of course, things are not quite so simple because the hybridization shift of the $\underline{c}d^9\underline{L}$ state in XPS is different from that of the $\underline{c}d^9$ state in XAS. We will address this problem more accurately below.

Since the XPS spectra have already been discussed in detail elsewhere, we concentrate on the cluster predictions for the XAS spectra. The final eigenstates and energies are determined by diagonalizing the Hamiltonian matrix,

$$H=\begin{vmatrix} 0 & T \\ T & \Delta+U-Q \end{vmatrix}, \tag{3}$$

taking as the zero of the energy of a $\underline{c}d^9$ configuration. The eigenvalues then are

$$E_{1,2}=\tfrac{1}{2}(\Delta+U-Q)\pm\tfrac{1}{2}[(\Delta+U-Q)^2+4T^2]^{1/2}, \tag{4}$$

and the satellite main-line separation

$$W=[(\Delta+U-Q)^2+4T^2]^{1/2}. \tag{5}$$

The eigenfunctions are given by

$$\begin{aligned} |\Psi_1\rangle&=\alpha_a|\underline{c}d^9\rangle+\beta_a|\underline{c}d^{10}\underline{L}\rangle, \\ |\Psi_2\rangle&=\beta_a|\underline{c}d^9\rangle-\alpha_a|\underline{c}d^{10}\underline{L}\rangle. \end{aligned} \tag{6}$$

Taking into account only transitions to d states, the intensities are given by

$$\begin{aligned} I_1&=(\sqrt{2}\alpha_0\alpha_a+\beta_0\beta_a)^2, \\ I_2&=(\sqrt{2}\alpha_0\beta_a-\beta_0\alpha_a)^2. \end{aligned} \tag{7}$$

Here the $\sqrt{2}$ arises from the two ways of getting from d^8 to $\underline{c}d^9$. The total intensity $(\beta_0^2+2\alpha_0^2)$ is equal to the total number of d holes in the ground state. From this we see that if the levels in the final state have the same ordering as in the *initial* state, the satellite intensity is low both because $\alpha_{0,a}>\beta_{0,a}$ and the destructive interference in the relation for I_2.

The next problem to discuss is the multiplet splitting and the apparent reduction with decreasing anion electronegativity. As we saw for the purely ionic calculation, the final-state configuration $\underline{c}d^9$ is composed of numerous states because of the atomic spin-orbit, Coulomb, and exchange interactions. However, the $\underline{c}d^{10}\underline{L}$ configuration has only two states, corresponding to a $2p_{1/2}$ and $2p_{3/2}$ hole. We also notice from Fig. 2 that the multiplet splitting in the $2p_{3/2}$ component is comparable in magnitude to the satellite main-line splitting. This causes the hybridization of the various $\underline{c}d^9$ states with the $\underline{c}d^{10}\underline{L}$ state to be different for each of the atomic $\underline{c}d^9$ states. We demonstrate this for a model in which we assume there to be two $\underline{c}d^9$ states belonging to different irreducible representations of the point group. Let the energies of these for the ion be $E(\Gamma_1)$ and $E(\Gamma_2)$. Each of these will mix with their initially degenerate configurations $\underline{c}d^{10}\underline{L}$ of Γ_1 and Γ_2 symmetry. The mixing will cause the apparent splitting between the $\underline{c}d^9$ Γ_1 and Γ_2 states to decrease if the energy of the $\underline{c}d^{10}\underline{L}$ state is higher than both of $\underline{c}d^9$ states. The reduction R in splitting for the main line is easily calculated by repeating the calculation of Eq. (4) for two representations, resulting in

$$R=\frac{1}{2}\left[1-\frac{\{[\Delta-E(\Gamma_1)+U-Q]^2+4T^2\}^{1/2}+\{[\Delta-E(\Gamma_2)+U-Q]^2+4T^2\}^{1/2}}{E(\Gamma_1)-E(\Gamma_2)}\right]. \tag{8}$$

This reduction of the multiplet splitting is shown pictorially in Fig. 4 and depends on the covalent mixing in the final state. We see from Eq. (8) that, for U, Q, and T constant, R decreases with decreasing Δ, as observed experimentally. It should be noted, however, that the reduction in multiplet splitting is a result of covalent mixing in the *final* state, which is considerably larger than that in the initial state, since $Q>U$.

Having explained the qualitative features of the spectra, we now turn to a more detailed comparison of theory and experiment. To do this we go one step further in the theory to take into account the large ligand hole bandwidth. This is necessary both to understand the band gaps in these materials[10] and to understand the rather broad satellite structure in the XAS spectra.

As we pointed out in a previous paper,[13] the Anderson impurity Hamiltonian[22] is considered appropriate for the problem of an isolated Ni impurity in the ligand matrix. Because the host band is initially full, we have only to cope with the two holes in the Ni d shell, for which, in principle, exact solutions can be obtained.

In order to calculate the ground state, we define a Hilbert space of two-hole configurations which transforms as the ${}^3A_{2g}$ irreducible representation with the assumption that there are no empty "host" states of importance,

$$|d^8\rangle=d_1d_2|\text{vac}\rangle, \tag{9a}$$

where $|\text{vac}\rangle$ is the filled ligand band and the filled d shell. We also have states with holes transferred to the ligand band,

$$|d^9\varepsilon\rangle=\frac{1}{\sqrt{2}}(d^\dagger_{1\uparrow}c_{\varepsilon 1\uparrow}+d^\dagger_{2\uparrow}c_{\varepsilon 2\uparrow})|d^8\rangle\ , \tag{9b}$$

$$|d^{10}\varepsilon\varepsilon'\rangle=\frac{1}{\sqrt{2}}d^\dagger_{1\uparrow}d^\dagger_{2\uparrow}(c_{\varepsilon 1\uparrow}c_{\varepsilon' 2\uparrow}+c_{\varepsilon 2\uparrow}c_{\varepsilon' 1\uparrow})|d^8\rangle\ , \tag{9c}$$

with $\varepsilon\le\varepsilon'$.

Here we adopted the short-hand notation $1=3z^2-r^2$ and $2=x^2-y^2$ for the d wave functions, while $d^\dagger_{i\sigma}$ creates an i,σ d electron and $c^\dagger_{\varepsilon i\sigma}$ creates an i,σ band electron with an energy ε. The diagonal matrix elements are then in analogy with the cluster model,

$$\begin{aligned}&\langle d^8|H|d^8\rangle=0\ ,\\ &\langle d^9\varepsilon|H|d^9\varepsilon'\rangle=\delta(\varepsilon-\varepsilon')(\Delta+\varepsilon)\ ,\\ &\langle d^{10}\varepsilon\varepsilon'|H|d^{10}\varepsilon''\varepsilon'''\rangle=\delta(\varepsilon-\varepsilon'')\delta(\varepsilon-\varepsilon''')\\ &\qquad\times(2\Delta+U+\varepsilon+\varepsilon')\ .\end{aligned} \tag{10}$$

We have the nonvanishing off-diagonal matrix elements

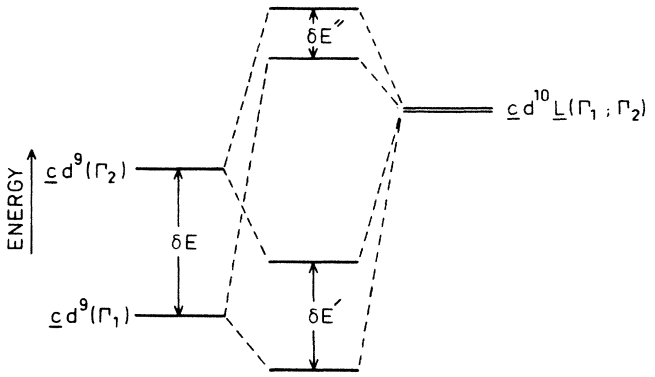

FIG. 4. Schematic energy diagram showing the influence of configuration interaction on the multiplet splitting. The multiplet splitting in the $\underline{c}d^9$ state is reduced by the mixing with the $\underline{c}d^{10}\underline{L}$ state. The reduction R is equal to $\delta E'/\delta E$.

$$\begin{aligned}&\langle d^8|H|d^9\varepsilon\rangle=\sqrt{2}V(\varepsilon)\ ,\\ &\langle d^9\varepsilon|H|d^{10}\varepsilon'\varepsilon''\rangle=\sqrt{2}V(\varepsilon)\delta(\varepsilon-\varepsilon')\delta(\varepsilon-\varepsilon'')+[1-\delta(\varepsilon'-\varepsilon'')][V(\varepsilon'')\delta(\varepsilon-\varepsilon')+V(\varepsilon')\delta(\varepsilon-\varepsilon'')]\ ,\end{aligned} \tag{11}$$

in which $V(\varepsilon)$ is the effective coupling between a d state and a ligand band state at ε. As long as the $|d^{10}\varepsilon\varepsilon'\rangle$ states are not important, but also not negligible, a good approximation can be found which simplifies the problem considerably.[13] In this approximation we define effective states $|d^{10}\varepsilon\varepsilon'\rangle$ such that

$$\langle d^9\varepsilon|H|d^{10}\varepsilon'\varepsilon''\rangle=\sqrt{2}V(\varepsilon'')\delta(\varepsilon-\varepsilon')\ , \tag{12}$$

and the full summation over ε' and ε'' has to be taken instead of $\varepsilon\le\varepsilon'$.

Writing now the ground state of the system as

$$|\Psi_0\rangle=A\left[|d^8\rangle+\int_{-W/2}^{W/2}a(\varepsilon)|d^9\varepsilon\rangle d\varepsilon+\int\int_{-W/2}^{W/2}b(\varepsilon,\varepsilon')|d^{10}\varepsilon\varepsilon'\rangle d\varepsilon\,d\varepsilon'\right]\ , \tag{13}$$

analytical expressions can be obtained for the coefficients A, $a(\varepsilon)$, and $b(\varepsilon,\varepsilon')$, as well as for hybridization energy δ, which is the energy lowering of the ground state due to hybridization with respect to $E(d^8)=0$. Expressions for these and for the ground-state occupation can be found in the Appendix of Ref. 13.

We now turn to the calculation of the XAS spectrum. We define the eigenstates of the two particle (core-hole, valence-hole) final state as $|\Psi_f(\Gamma_m(n))\rangle$ being the configuration-interaction eigenstate Ψ_f transforming as the nth component of the irreducible representation Γ_m. For a random orientation of the magnetic moment we can write, for the spectral function of x-ray absorption,

$$\rho^\alpha_{\rm XAS}(\omega)=\frac{1}{\pi}{\rm Im}G^\alpha_{\rm XAS}(z),\quad z=\omega-iy \tag{14}$$

with

$$G^\alpha_{\rm XAS}(z)=\sum_{M_S,\alpha,m,n}\langle\Psi_0(M_S)|P^*_\alpha G(\Gamma_m(n))P_\alpha|\Psi_0(M_S)\rangle\ , \tag{15}$$

where P_α is the dipole operator for light with polarization α and $|\Psi_0(M_S)\rangle$ is the ground-state wave function with magnetic quantum number M_S.

The Green's-function operator $G(\Gamma_m(n))$ is defined as

$$G(\Gamma_m(n))=\sum_f|\Psi_f(\Gamma_m(n))\rangle\frac{1}{z+\delta-E_f(\Gamma_m(n))}\times\langle\Psi_f(\Gamma_m(n))|\ , \tag{16}$$

with δ being the ground-state energy and $E_f(\Gamma_m(n))$ the eigenvalue of Ψ_f.

Let us first consider the case where we can neglect configuration interaction, i.e., $\Delta\gg V$. The ground state can be written as $|d^8(^3A_{2g});M_S\rangle$ and the final states as $|\underline{c}d^9(\Gamma_m(n))\rangle$. In this case Γ_m labels the multiplets of the $|\underline{2p}3d^9\rangle$ configuration and $E(\Gamma_m)$ are the multiplet energies. Defining the transition matrix element as

$$t(^3A_{2g}(M_S);\alpha;\Gamma_m(n))=\langle\Psi_0(M_S)|P_\alpha|\Psi(\Gamma_m(n))\rangle\ , \tag{17}$$

Eq. (15) reduces to the expression for the multiplet spectrum,

$$G_{\rm XAS}(z)=\sum_{M_S,\alpha,m,n}\frac{|t(^3A_{2g}(M_S);\alpha;\Gamma_m(n))|^2}{z+\delta-E(\Gamma_m)}\ , \tag{18}$$

the results of which were already discussed (see also Fig. 2).

Generally speaking, the inclusion of configuration interaction introduces a much more complicated problem, as, for instance in the calculation of Fujimori *et al.* of the valence photoemission spectrum in the cluster approximation.[9] Fortunately, this is not the case for the present problem due to the fact that the multiplet-split $|2\underline{p}3d^9\rangle$ states are coupled only to $|2\underline{p}3d^{10}\varepsilon\rangle$ states. Because the d shell is filled in the latter state, and the interaction between the $2p$ hole and the ligand hole can be safely assumed to be negligible, it is possible to construct $|2\underline{p}3d^{10}\underline{L}\rangle$ states such that the configuration-interaction problem is diagonal with respect to the Coulomb and exchange interactions. The basic reason is that the $|2\underline{p}3d^{10}\varepsilon\rangle$ states can be freely rotated, being independent, such that they are of the same symmetry $\Gamma_m(n)$ as the $|2\underline{p}d^9\rangle$ states. More explicitly, we can write, for the $|2\underline{p}d^9\rangle$ states,

$$|2\underline{p}d^9;\Gamma_m(n)\rangle=\sum_{j,m_j,\nu,\sigma}\alpha^{mn}_{jm_j\nu\sigma}d_{\nu\sigma}p_{jm_j}|0\rangle\ , \tag{19}$$

with ν labeling an e_g or t_{2g} d orbital and p_{jm_j} annihilating a core electron in j, m_j. Because of the independency of the $|2\underline{p}d^{10}\varepsilon\rangle$ states, we are free to construct states

$$|2\underline{p}d^{10}\varepsilon;\Gamma_m(n)\rangle=\sum_{j,m_j,\nu,\sigma}\alpha^{mn}_{jm_j\nu\sigma}c_{\varepsilon\nu\sigma}p_{jm_j}|0\rangle\ , \tag{20}$$

such that the nondiagonal matrix elements have the following simple form:

$$\langle 2\underline{p}d^9;\Gamma_m(n)|H|2\underline{p}d^{10}\varepsilon;\Gamma_{m'}(n')\rangle=\delta_{mm'}\delta_{nn'}V(\varepsilon)\ . \tag{21}$$

Furthermore, we have the diagonal matrix elements of the configuration-interaction problem, with respect to $E_j=E(2\underline{p}_j3d^9)$,

$$\langle 2\underline{p}d^9;\Gamma_m(n)|H|2\underline{p}d^9;\Gamma_{m'}(n')\rangle=\delta_{mm'}\delta_{nn'}(E_j+E(\Gamma_m))\ , \tag{22}$$

$$\langle 2\underline{p}d^{10}\varepsilon;\Gamma_m(n)|H|2\underline{p}d^{10}\varepsilon';\Gamma_{m'}(n')\rangle=\delta_{mm'}\delta_{nn'}\delta(\varepsilon-\varepsilon')[\Delta-Q+U+\varepsilon+E_j+E'(\Gamma_m)]\ . \tag{23}$$

E_j is the energy of the $j=\frac{3}{2},\frac{1}{2}$ core hole and $E(\Gamma_m),E'(\Gamma_m)$ are defined with respect to these energies. In Eq. (22), $E(\Gamma_m)$ corresponds to the multiplet energies of the $|2\underline{p}3d^9\rangle$ configuration.

In the derivation of these equations we made an approximation which, in principle, can influence the fine structure of the spectrum. This concerns the treatment of the crystal-field splitting of the e_g- and t_{2g}-type d orbitals. In Eq. (20) it is implicitly assumed that the hybridization of e_g and t_{2g} electrons is the same, and the crystal-field splitting enters as an electrostatic contribution raising the energy of the t_{2g} d hole [in Eqs. (22) and (23), $\varepsilon_d=\varepsilon_d(e_g)$, and $10Dq$ is absorbed in $E(\Gamma_m)$].

It is, however, well known that a large part of the crystal-field splitting is due to covalency[23] and calculations show that typically $V_{e_g}(\varepsilon)\simeq 2V_{t_{2g}}(\varepsilon)$.[24] Taking this into account, Eq. (20) is no longer valid which severely complicates the problem, although it is still solvable using recently developed two-particle Green's-function techniques.[25,26]

It is, however, also well known that the electrostatic model is a very good approximation to the full ligand field problem. Employing a cluster calculation, this is relatively easy to check for this special case, and we found from this that, for all values of $\Delta-Q+U$, the electrostatic model exhibits essentially the same results as the ligand field model with $10Dq\simeq 1$ eV and $V_{e_g}(\varepsilon)\simeq 2V_{t_{2g}}(\varepsilon)$.

In the energies of the $|2\underline{p}d^{10}\varepsilon\rangle$ states [Eq. (23)] we also included a shift $E'(\Gamma_m)$ due to transformation of Eq. (20). The reason is that due to the exchange and Coulomb interactions some $2p_{3/2}$ character will be mixed into the $2p_{1/2}$ manifold and vice versa, the amount of which depends on the particular Γ_m. These intermediate-coupling effects are very weak for the Ni ion due to the large spin-orbit coupling and we ignored this shift of the $|2\underline{p}^{10}\varepsilon\rangle$ states, although we did take intermediate coupling into account in the calculation of the $|2\underline{p}3d^9\rangle$ multiplet spectrum.

Having found the right representation for the final state, we now have to express the Green's function in this basis. Because we have diagonalized the multiplet problem, we can write Eq. (15) as

$$G_{\mathrm{XAS}}=\sum_{M_S,\alpha,m,n}|t(^3A_{2g}(M_S);\alpha;\Gamma_m(n))|^2 g(\Gamma_m(n))\ , \tag{24}$$

which means that we can solve the configuration-interaction problem as contained in $g(\Gamma_m(n))$ for each multiplet separately, while the spectrum is given by the sum of these multiplied by the transition matrix element from the $^3A_{2g}$ ground state to the particular Γ_m.

Using Eq. (10), we can express $g(\Gamma_m(n))$ as

$$g(\Gamma_m(n))=A^2\left[G^{2\underline{p}d^9}_{2\underline{p}d^9}(\Gamma_m)+\frac{1}{\sqrt{2}}\int[a(\varepsilon)G^{2\underline{p}d^{10}\varepsilon}_{2\underline{p}d^9}(\Gamma_m)+\mathrm{H.c.}]d\varepsilon+\tfrac{1}{2}\int a^*(\varepsilon)a(\varepsilon')G^{2\underline{p}d^{10}\varepsilon'}_{2\underline{p}d^{10}\varepsilon}(\Gamma_m)d\varepsilon\,d\varepsilon'\right]\ , \tag{25}$$

where the G^j_i's (i,j $|2\underline{p}d^9\rangle$, $|2\underline{p}d^{10}\varepsilon'\rangle$) are defined by

$$G^j_i(\Gamma_m)=\left\langle i\left|\frac{1}{z+\delta-H(\Gamma_m)}\right|j\right\rangle\ , \tag{26}$$

with $H(\Gamma_m)$ defined by Eqs. (21)–(23). Note that we incorporated in Eq. (25) a factor $1/\sqrt{2}$ for the transition $|d^9\varepsilon\rangle \rightarrow |\underline{2p}d^{10}\varepsilon\rangle$ in order to account for the two ways of getting from $|d^8\rangle \rightarrow |\underline{2p}d^9\rangle$, which is, of course, independent of the irreducible representation. Using straightforward matrix-inversion techniques or Dyson equations to solve for the $G_i^j(\Gamma_m)$, we find

$$g(\Gamma_m(n))=A^2\left[\left[1-\frac{1}{\sqrt{2}}B(\Gamma_m)\right]G^{\underline{2p}d^9}_{\underline{2p}d^9}(\Gamma_m)+\tfrac{1}{2}C(\Gamma_m)\right], \tag{27}$$

with

$$B(\Gamma_m)=\int \frac{a^*(\varepsilon)V(\varepsilon)d\varepsilon}{z+\delta+Q-\Delta-U-\varepsilon-E_j}, \tag{28}$$

$$C(\Gamma_m)=\int \frac{|a(\varepsilon)|^2 d\varepsilon}{z+\delta+Q-\Delta-U-\varepsilon-E_j}, \tag{29}$$

and

$$G^{\underline{2p}d^9}_{\underline{2p}d^9}(\Gamma_m)=\frac{1}{z+\delta-E_j-E(\Gamma_m)-\int \frac{|V(\varepsilon)|^2 d\varepsilon}{z+\delta+Q-\Delta-U-\varepsilon-E_j}}. \tag{30}$$

Note that $G^{\underline{2p}d^9}_{\underline{2p}d^9}(\Gamma_m)$, which is representative for the final-state dynamics, describes a local $|\underline{p}d^9\rangle$ state coupled to a single continuum $|\underline{p}d^{10}\varepsilon\rangle$. The factors $B(\Gamma_m)$ are due to the occupancy of $|d^9\varepsilon\rangle$ states in the ground state. Although Eq. (30) can be represented analytically for a model density of states, this is not true for Eqs. (28) and (29) because of the difficult form of $a(\varepsilon)$.

In Fig. 5 we have schematically outlined the energetics of the ground state and the final state after x-ray absorption. The ligand hole density of states was simulated by a semielliptical band having a width of 3 eV. The ground-state properties are discussed in great detail in Ref. 13. Due to the large width of the multiplet structure of the $|\underline{2p}d^9\rangle$, some of its states may fall outside the $|\underline{2p}d^{10}\varepsilon\rangle$ continuum, as depicted graphically in Fig. 5.

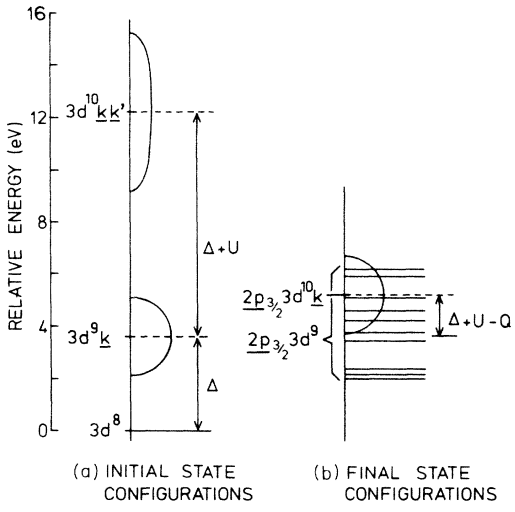

FIG. 5. Schematic representation of the energy of the different configurations for (a) the initial and (b) final states in the L_3 absorption for the case of $NiCl_2$. Configurations with a ligand hole ($\underline{k}$) have a bandwidth W. The $2\underline{p}_{3/2}3d^9$ configuration is multiplet-split. Not drawn is the mixing between the configurations.

V. COMPARISON WITH EXPERIMENT

In the XPS paper[13] we argued that Q, U, and $\int_{-W/2}^{W/2}V^2(\varepsilon)d\varepsilon$ are approximately constant for the dihalides. Also, we know that Q and U must be around 7 and 5 eV, respectively, in order to obtain the observed satellite energies in XPS and also in XAS. We are then left with only one adjustable parameter for the dihalides (Δ).

In Fig. 6 we show the calculated XAS spectra together with the experimental data using the parameters as listed in Table II and the theory presented in the preceding section. We see that the agreement with experiment is quite good. The theory reproduces very well the reduction in multiplet splitting on going to less electronegative anions. We obtain the expected trend in the charge-transfer energies (Δ), which are consistent with the values obtained by $2p$ XPS, and the theory reproduces the satellite structure quite nicely. There still is a problem with the shape of the satellite structure, which is not reproduced in detail by theory. This, however, could be due to an oversimplified ligand hole density of states. It is known from band-structure calculations that the ligand p band density of states actually is composed of a two-peaked structure rather than a single broad band. Although we could include this in the theory, it would complicate the numerics and not really add any new physics.

In comparing the parameters of Table II with those of the XPS results,[13] we notice that the only large difference is in the values for T. As pointed out in the XPS paper, this is not unexpected in view of the fact that off-diagonal Coulomb interactions involving the core hole have been neglected.

For comparison, we also performed a calculation in the limit of zero bandwidth ($W \rightarrow 0$), where the impurity model changes into the cluster model. In the cluster model the sum of the multiplet splittings in both interacting final states is constant for a given irreducible representation (see Fig. 4). In a specific final state the reduction of the multiplet from its bare value is obtained from Eq. (8) and is roughly equal to the amount of $2\underline{p}3d^9$ character in that state. This is also true in the impurity model, ex-

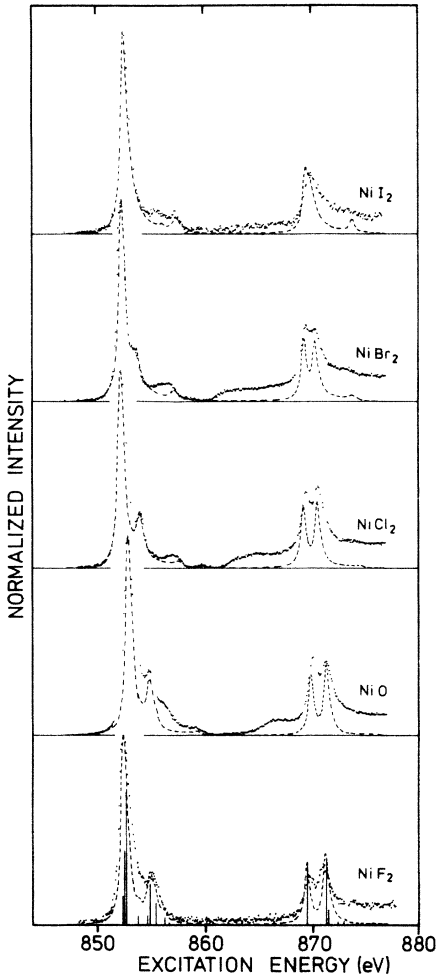

FIG. 6. Calculated x-ray-absorption spectra (dashed line) using the described impurity model, with parameters as listed in Table II, compared to the experimental spectra (dots).

cept when $\Delta+U-Q$ becomes too small or even negative. In these cases the lowest eigenvalues of all irreducible representations are pinned to the low-energy threshold of the $|\underline{c}d^{10}\underline{L}\rangle$ continuum because a bound state can no longer be pushed out of this by the interaction with a $|\underline{c}d^{9}\rangle$ state.

To show the significance of this effect, we compare in Fig. 7 the impurity model result for NiI_2 ($\Delta=1.5$ eV) with the result obtained from cluster theory using the same parameters. In the cluster result the main line is

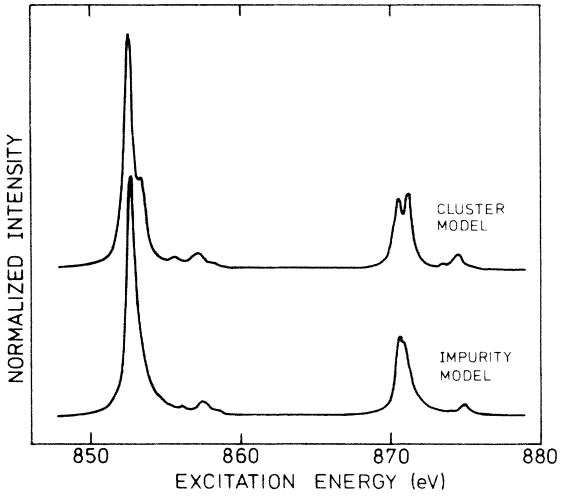

FIG. 7. Cluster model and impurity model compared for the case of NiI_2 ($\Delta=1$ eV).

still split up, and it turns out that in order to decrease this splitting down to less than the experimental resolution, one needs $\Delta\lesssim 0$, which is very unlikely. On the other hand, the impurity result yields a single slightly asymmetric line, with a threshold corresponding to the $|\underline{c}d^{10}\underline{L}\rangle$ continuum threshold. As can be seen in Fig. 6 this line shape is in perfect agreement with the experimental result.

As we argued in Sec. III, the difference between XPS and XAS threshold lines is due to the ligand ionization potential ε_L. By comparing results from the XPS paper[13] with results from this paper, quantitative estimates for the ε_L values of the dihalides can be derived. In Table III values are given for the energy of the $|2\underline{p}_{3/2}d^{9}\rangle$ configuration, as obtained from the fits in Fig. 6. As expected, these values vary only slightly in the series.

In Table III we reproduced the energies for the $|2\underline{p}_{3/2}d^{8}\rangle$ configuration as found from the analysis of the XPS spectra, which are also approximately constant. From these numbers and from the values of Δ and Q, as listed in Table II, it is possible to calculate the energy of the $|2\underline{p}_{3/2}d^{9}\underline{L}\rangle$ configuration, which is

$$E(2\underline{p}_{3/2}d^{9}\underline{L})=E(2\underline{p}_{3/2}d^{8})+\Delta-Q\ . \tag{31}$$

The ligand ionization potential is then given by

$$\varepsilon_L=E(2\underline{p}_{3/2}d^{9}\underline{L})-E(2\underline{p}_{3/2}d^{9})\ . \tag{32}$$

TABLE III. Absolute energy positions (eV) of configurations in the presence of the core hole as derived in this paper [$E(2\underline{p}_{3/2}d^{9})$] and from XPS [$E(2\underline{p}_{3/2}d^{8}),E(2\underline{p}_{3/2}d^{9}\underline{L})$] (Ref. 13). In addition, we list values for the ligand ionization energy ε_L as derived from a combination of XPS and XAS.

	$E(2\underline{p}_{3/2}d^{9})$	$E(2\underline{p}_{3/2}d^{8})$	$E(2\underline{p}_{3/2}d^{9}\underline{L})$	ε_L
NiI_2	853.7	860.6	855.1	1.4
$NiBr_2$	853.3	860.5	856.1	2.8
$NiCl_2$	853.3	860.4	857.0	3.7
NiF_2	853.6	859.8	859.3	5.7

As can be seen from Table III, ε_L as derived in this way shows the expected trend as a function of the anion electronegativity.

These numbers are rather large and constitute, in fact, the better part of the charge-transfer energy $\Delta=\varepsilon_d+\varepsilon_L$. This is, however, consistent with recent results of Huefner derived from photoemission and optical data.[7] As we showed,[10] the band gap in these materials is determined approximately by Δ, while the first electron-affinity state is at $\simeq\varepsilon_d$ from the Fermi level E_F and the first ionization state is at $\simeq\varepsilon_L$ from E_F. As can be seen from Huefner's results, E_F is very close to the first affinity state for $NiBr_2$ and $NiCl_2$, pointing to a relatively large ε_L. More detailed calculations including covalency show that the values of ε_L as presented in Table III are close to the values needed to pinpoint the Fermi level at the correct position in the gap.

We now turn to the problem of the continuum edge so clearly visible in the $2p_{3/2}$ region of $NiBr_2$, $NiCl_2$, and NiO. It is fairly obvious that this continuum structure is due to transitions from $2p$- to $4s$-like states. If the $4s$ electron were completely decoupled from the remaining system (core-hole and d and ligand electrons), we should, in fact, see three continuum thresholds corresponding to the three final states seen in XPS.[27] The basis states used to describe the continuum absorption would be of the form $\underline{c}d^8k$, $\underline{c}d^9\underline{L}k$, and $\underline{c}d^{10}\underline{L}^2k$, which are just the XPS basis states with a continuum electron added. These continuum states are graphically depicted in Fig. 8 for the $NiCl_2$ case. Just as in XPS, these states will be coupled because of the local transfer integrals

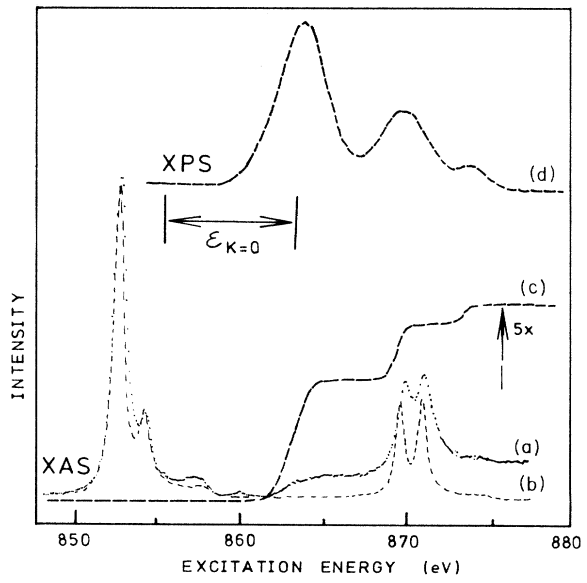

FIG. 8. Decomposition of (a) the of XAS spectrum into (b) excitations to local final states and (c) excitations to continuum states (5× enhanced energy scale) for $NiCl_2$. The three XAS continuum edges $\underline{c}d^9\underline{L}k$, $\underline{c}d^{10}\underline{L}^2k$, and $\underline{c}d^8k$, respectively, are obtained using (d) the XPS energy positions shifted by $\varepsilon_{k=0}$ from the final states $\underline{c}d^9\underline{L}$, $\underline{c}d^{10}\underline{L}^2$, and $\underline{c}d^8$, respectively, and their relative intensities. Note the high resolution of XAS compared to XPS.

$$\langle \underline{c}d^8k \mid H \mid \underline{c}d^9\underline{L}k' \rangle = \sqrt{2}T\delta_{kk'} ,$$
$$\langle \underline{c}d^9\underline{L}k \mid H \mid \underline{c}d^{10}\underline{L}^2k' \rangle = \sqrt{2}T\delta_{kk'} , \tag{33}$$

where the $\delta_{kk'}$ arises from the assumption that the continuum electron is decoupled from the system left behind, which is equivalent to the sudden approximation in XPS. From this we see that we expect three continuum thresholds with the same energy separation as the peaks observed in XPS, but shifted up in energy by $\varepsilon_{k=0}$, which is just the $4s$ threshold energy. The lowest-energy threshold will—according to the XPS analysis—correspond to a predominantly $\underline{c}d^9\underline{L}k$ continuum. The energy of this relative to the predominantly $\underline{c}d^9$ XAS main line is therefore a measure of $\varepsilon_{\underline{L}}+\varepsilon_k$, neglecting the small difference in hybridization shifts. $\varepsilon_{\underline{L}}+\varepsilon_k$ determined in this way is 9 eV for $NiBr_2$ and 10 eV for $NiCl_2$. These values are 1.3 and 0.7 eV larger than the recently determined energies of the Γ excitons from optical experiments.[31] Correcting these for the exciton binding energies $\sim$0.5—2 eV, we see that the optical and XAS results are in good agreement. In fact, the small peaks observed in $NiCl_2$ between c and d (Fig. 1) could be due to the same Γ exciton observed optically. Its energy relative to the continuum threshold is about 1.7 eV in $NiCl_2$ and 1.5 eV in $NiBr_2$, which are reasonable values for exciton binding energies.

As can be seen from Fig. 6, the overall agreement between experiment and theory is somewhat worse for the $2p_{1/2}$ spectrum than for the $2p_{3/2}$ spectrum. In the first place, we notice that the $2p_{1/2}$ spectrum is more broadened than the $2p_{3/2}$ lines, which is certainly due to the Coster-Kronig decay channel. Moreover, the comparison between theory and experiment in Fig. 6 suggests a Fano profile[28] for the $2p_{1/2}$ lines. This is well known from the analysis of the $3d_{3/2}$ white line of the rare earths,[29] and is due to coherent optical excitation of the $2p_{1/2}$ states and the $2p_{3/2}$ continua, which are mutually coupled by Coster-Kronig matrix elements.

We showed recently in a separate paper[30] that under certain conditions it is not possible to separate the inductive screening of the core hole and its decay. We showed there that Coster-Kronig decay channels are candidates for these interference effects and that, in fact, the large difference between the $2p_{1/2}$ and $2p_{3/2}$ XPS lines can be traced back to such a cause. This interference primarily affects satellite—versus—main-line intensities and line shapes. As can be seen from Fig. 6, the theory indeed seems to overestimate the $2p_{1/2}$ satellite strength, which points to such an effect. However, the effects are small and a detailed theoretical explanation would be quite difficult, and we would emphasize at this point the main conclusion of the interference paper, namely that it is better to look at $2p_{3/2}$ spectra than at the more complicated $2p_{1/2}$ spectra.

VI. CONCLUSIONS

In this paper we have shown that the threshold structure in the $L_{2,3}$ absorption is due to multiplet structure. Increase of the covalent mixing in the final state results in a reduction of the multiplet structure and in the appearance of screening satellites. Cluster model calculations

are compared to those of an impurity model. In the case of NiI_2 the latter model is in better agreement with the observed reduction in the multiplet splitting. The position of the $4s$ continuum edge is in good agreement with the energies of the Γ excitons from optical experiments.

We have shown that the XAS spectra of Ni dihalides and NiO can be understood using the same theory and nearly the same parameters as are used to interpret the XPS spectra. The fact that in XPS large satellites are observed together with the very-low-intensity satellites in XAS is direct evidence for large d-d Coulomb interactions and core-hole—d interactions of comparable magnitude. In XPS the changes in ground-state covalency with anion electronegativity are observed in changes in the "screened" core-hole binding energy, as well as in changes in the satellite structure. In XAS the changes in covalency are primarily seen in changes in the multiplet splittings although small changes in satellite intensities are observed. We have shown that the large differences between XPS and XAS can be quantitatively understood within the same theoretical framework.

Although a detailed analysis of XPS and XAS spectra can yield quite consistent values of parameters in a model Hamiltonian, we stress that these values need not, in general, be equal to those required to describe the ground state and low-energy spectroscopies, although they are expected to show the same trends and be of the same relative magnitude.

An example of experiment dependent parameters is the small transfer integral T needed for XAS in comparison to XPS (1.5 versus 2 eV), which can be traced to the oversimplification of the core-hole potential as pointed out in the XPS paper.[13] Also, the values of U and Δ are effective parameters, which again include effects (not *explicitly* considered) of the core-hole potential, such as nearest-neighbor Coulomb interactions, which are not present in the ground state or in low-energy spectroscopies.

ACKNOWLEDGMENTS

We are grateful to the Laboratoire pour l'Utilisation du Rayonnement Electromagnetique (LURE) technical staff for their valuable aid. This work was supported by the Netherlands Foundation for Chemical Research (Stichting Scheikundig Onderzoek Nederland), with financial aid from the Netherlands Organization for the Advancement of Pure Research (Stichting Zuiver Wetenschappelijk Onderzoek), and by the Centre Nationale de la Recherche Scientifique (CNRS), France.

[1]S. H. de Boer and E. J. W. Verwey, Proc. Phys. Soc. London, Sect. A **49**, 59 (1937).
[2]A. H. Wilson, Proc. Soc. London, Sect. A **133**, 458 (1931).
[3] N. F. Mott, Proc. Phys. Soc. London, Sect. A **62**, 416 (1949).
[4]K. Terakura, A. R. Williams, T. Oguchi, and J. Kuebler, Phys. Rev. Lett. **52**, 1830 (1984).
[5]K. Terakura, T. Oguchi, A. R. Williams, and J. Kuebler, Phys. Rev. B **30**, 4734 (1984).
[6]G. A. Sawatzky and J. W. Allen, Phys. Rev. Lett. **53**, 2339 (1984).
[7]S. Huefner, Solid State Commun. **53**, 707 (1985).
[8]S. Antoci and L. Mihich, Phys. Rev. B **18**, 5768 (1978); **21**, 3383 (1980).
[9]A. Fujimori and F. Minami, Phys. Rev. B **30**, 957 (1984); A. Fujimori, F. Minami, and S. Sugano, *ibid.* **29**, 5225 (1984).
[10]J. Zaanen, G. A. Sawatzky, and J. W. Allen, Phys. Rev. Lett. **55**, 418 (1985); J. Magn. Magn. Mater. **54-57**, 607 (1986).
[11]G. van der Laan, C. Westra, C. Haas, and G. A. Sawatzky, Phys. Rev. B **23**, 4369 (1981).
[12]G. A. Sawatzky, in *Studies in Solid State Chemistry,* edited by R. Metselaar (Elsevier, Amsterdam, 1982), Vol. 3, p. 3.
[13]J. Zaanen, C. Westra, and G. A. Sawatzky (unpublished).
[14]B. T. Thole, R. D. Cowan, G. A. Sawatzky, J. Fink, and J. C. Fuggle, Phys. Rev. B **31**, 6856 (1985).
[15]M. Lemmonnier, O. Collet, C. Depautex, J.-M. Esteva, and D. Raoux, Nucl. Instrum. Methods **152**, 109 (1978).
[16]T. Yamaguchi, S. Shibuya, S. Suga, and S. Shin, J. Phys. C **15**, 2641 (1982).
[17]G. van der Laan, J. Zaanen, G. A. Sawatzky, R. Karnatak, and J.-M. Esteva, Solid State Commun. **56**, 673 (1985).
[18]A self-consistent relativistic Hartree-Fock calculation has been performed by B. T. Thole (unpublished).
[19]G. van der Laan, Solid State Commun. **42**, 165 (1982).
[20]A. Fujimori, Phys. Rev. B **28**, 4489 (1983).
[21]E. Wuilloud, H. R. Moser, W.-D. Schneider, and Y. Baer, Phys. Rev. B **28**, 7354 (1983).
[22]O. Gunnarsson and K. Schönhammer, Phys. Rev. B **28**, 4315 (1983).
[23]A. J. H. Wachters and W. C. Nieuwpoort, Phys. Rev. B **5**, 4291 (1972).
[24]L. F. Mattheiss, Phys. Rev. B **5**, 290, 306 (1972).
[25]M. Vos, D. van der Marel, and G. A. Sawatzky, Phys. Rev. B **29**, 3073 (1984).
[26]J. Zaanen, G. A. Sawatzky, J. Fink, W. Speier, and J. C. Fuggle, Phys. Rev. B **32**, 4906 (1985).
[27]T. Jo and A. Kotani have recently formulated an eleborate theory about the L_3 edge of CeO_2. Here the interaction between the p hole and f electron with the $5d$ electron is considerable and they find strong deviations from the XPS shape convoluted with the $5d$ unoccupied density of states. However, if the bandwidth of the excited electron is much larger than the interaction with the core hole, the proposed procedure is essentially right [T. Jo and A. Kotani, Solid State Commun. **54**, 451 (1985)].
[28]U. Fano, Phys. Rev. **124**, 1866 (1961).
[29]B. T. Thole, G. van der Laan, J. C. Fuggle, G. A. Sawatzky, R. Karnatak, and J. M. Esteva, Phys. Rev. B **32**, 5107 (1985).
[30]J. Zaanen and G. A. Sawatzky (unpublished).
[31]W. Folkerts and C. Haas, Phys. Rev. B **32**, 2559 (1985).